Electronic Supplementary Material (ESI) for Journal of Materials Chemistry C.

Supporting Information

Synthesis of Millimeter Sized $Mo_xW_{(1-x)}S_{2y}Se_{2(1-y)}$ Monolayer Alloys with Adjustable Optical and Electrical Properties and Their Magnetic Doping

You Li[1,2], Yiwen Wang[1], Sabir Hussain[2], Liming Xie[2] and Junjie Qi[1*]

[1] *School of Materials Science and Engineering, University of Science and Technology Beijing, Beijing 100083, PR China*

[2] *School of Nanoscience and Technology, University of Chinese Academy of Sciences, Beijing 100049, PR China*

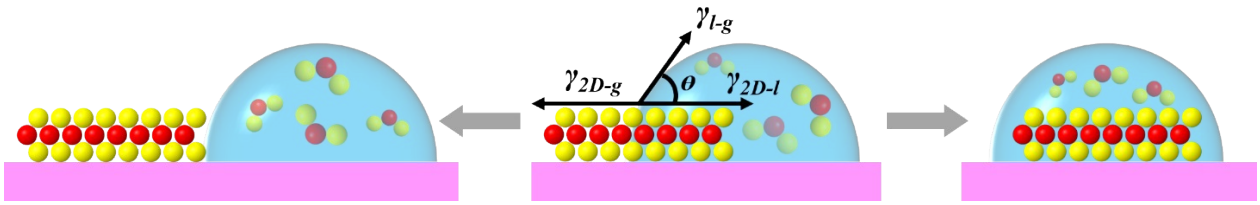

Fig. S1. Our LPEE purposed mechanism: the droplet horizontally displaces to maximize higher surface tension and induces the self-limited monolayer growth.

As shown in Fig. S1, based on Young's equation, when the droplet is in the non-wetting state, the following equations are satisfied:

$$\gamma_{l\text{-}g} > \frac{\gamma_{2D\text{-}g} - \gamma_{2D\text{-}l}}{\cos\theta} \#(1)$$

$\gamma_{l\text{-}g}$ is the surface tension of the solution, $\gamma_{2D\text{-}g}$ is the surface tension of the 2D material, $\gamma_{2D\text{-}l}$ is the surface tension between the 2D material and the solution, and θ is the contact angle of the droplet above the 2D material.[1-2] The greater the surface tension of the solution, the more favorable to make the droplet in a non-wetting state. Because the surface energy of the TMD alloys in the droplet is higher than that of the TMD alloys outside the droplet, the droplet shrinks inward, making the TMD alloys outside the droplet, and thus reducing the surface energy. The thickness of the precipitated transition metal disulfide will not increase again, i.e., the precipitated TMD alloys will not grow vertically, but only horizontally, because there is no source of supply of the precipitated transition metal disulfide vertically, but only horizontally, and thus a self-limiting growth behavior is achieved. An alkali metal halide salt was chosen as the solvent, its saturation vapor pressure is much higher than

that of TMD alloys. So, the possibility of salt volatilization is high, a certain amount of salt volatilizes the solution to supersaturation, will reach the state of supersaturation, and then precipitate TMD alloys. The thickness of the precipitated TMD alloys is determined by the degree of supersaturation of the TMD alloys in the solution. If the supersaturation is large, the precipitated TMD alloys are multilayers. If the supersaturation is small, precipitated TMD alloys are monolayers. Since the $Mo_xW_{1-x}S_{2y}Se_{2(1-y)}$ alloys are less supersaturated in solution, the crystals produced are monolayer.

During the growth process, the salt has a high vapor pressure, causing the salt to continuously volatilize to the substrate surface. As the salt is mixed with the precursor, begins to volatilize with the precursor and adsorbs on the surface of the substrate, becoming a solution. At this point, because the salt has a high saturation vapor pressure, the salt volatilizes from the solution and the alloy reaches supersaturation, which precipitates on the surface of the solution. As the salt continues to evaporate, as-grown alloys also continue to precipitate, and the size of as-grown alloys continues to increase, while the size of the solution continues to decrease until it disappears. At the same time, due to the larger surface tension of CsCl (75 mN/m), the driving force for the solution to move forward is high, so that the lateral size of the alloy increases continuously, and millimeter-scale $Mo_xW_{1-x}S_{2y}Se_{2(1-y)}$

monolayer is achieved.

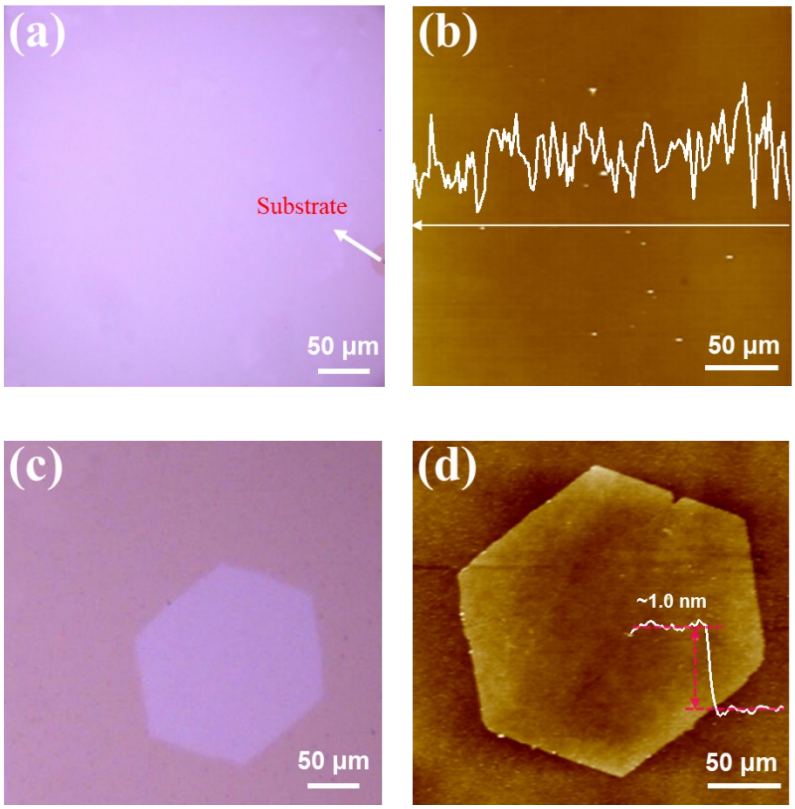

Fig. S2 AFM images of $Mo_xW_{(1-x)}S_{2y}Se_{2(1-y)}$ monolayers. (a-b) Optical image and AFM image of the alloy film. (c-d) Optical image and AFM image of the area near the edge of an alloy film, showing hexagonal monolayer islands (top, ~ 1 nm in height) that merge into a continuous film (bottom).

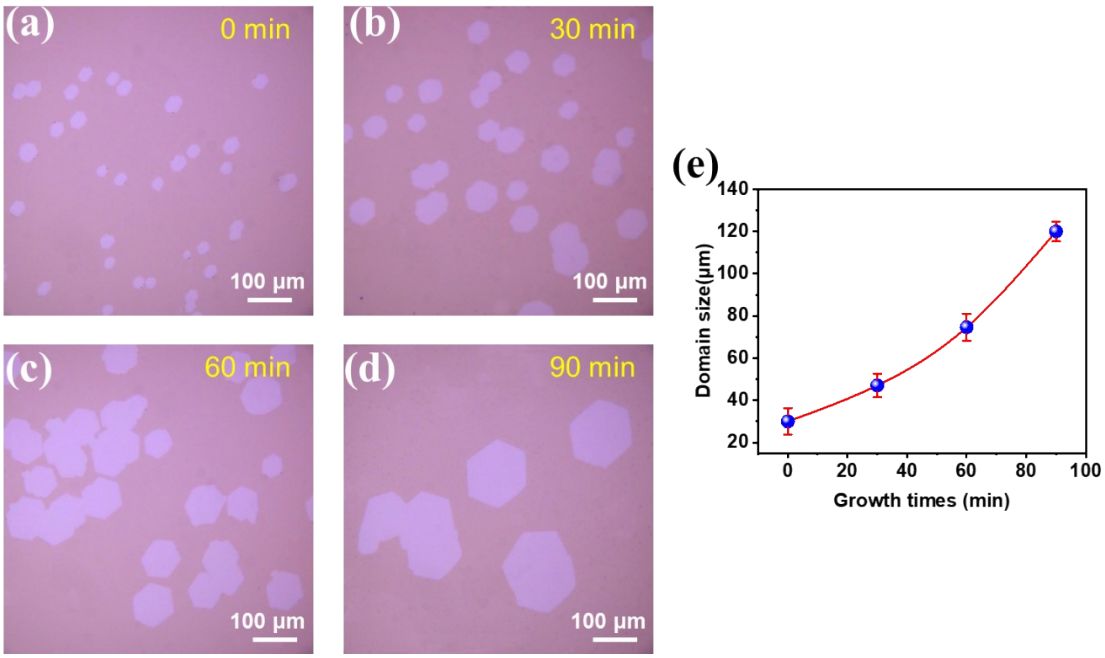

Fig. S3 LPEE of $Mo_xW_{(1-x)}S_{2y}Se_{2(1-y)}$ monolayers at different growth times. (a-d) Optical images

of as-grown $Mo_xW_{(1-x)}S_{2y}Se_{2(1-y)}$ with different growth times. (e) A function of the growth time dependent domain size for $Mo_xW_{(1-x)}S_{2y}Se_{2(1-y)}$ monolayers.

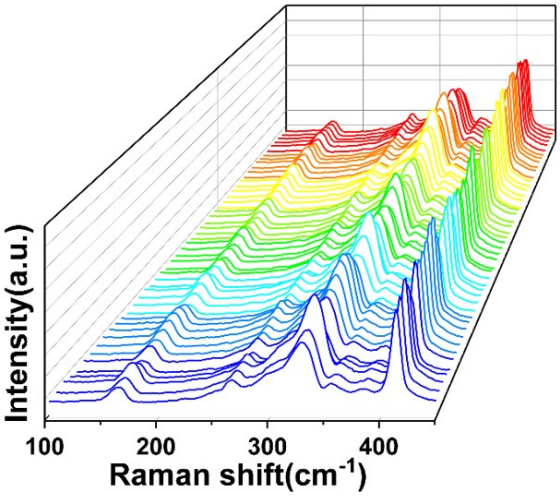

Fig. S4 Raman spectra of the $Mo_xW_{(1-x)}S_{2y}Se_{2(1-y)}$ film collected from 50 various positions.

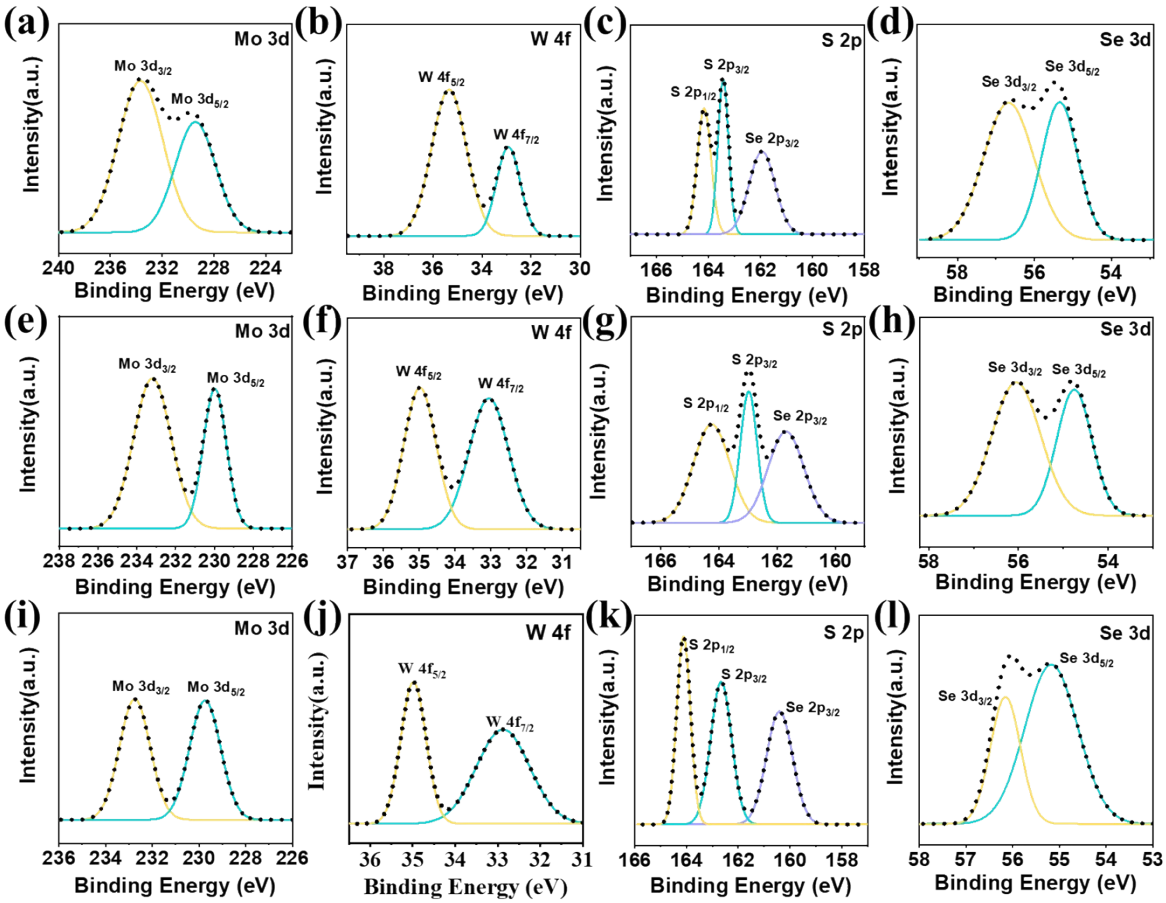

Fig. S5 XPS spectra of as-grown $Mo_xW_{(1-x)}S_{2y}Se_{2(1-y)}$ monolayers at (a-d) 825°C, (e-h) 850°C, (i-l) 875 °C, revealing the 3d, 4f, 2p and 3d binding states of Mo, W, S and Se respectively.

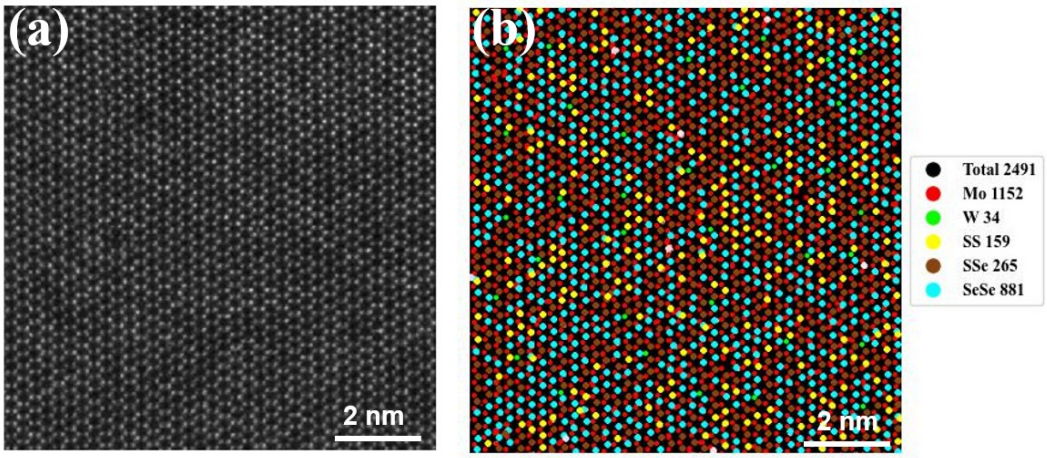

Fig. S6 (a) HAADF-STEM images of the as-grown $Mo_xW_{(1-x)}S_{2y}Se_{2(1-y)}$ monolayer at 825℃. (b) Related atom-labeled image (red – Mo, green – W, SS – yellow, SSe – brown, and SeSe – blue) that indicates uniform distribution of elements in the $Mo_xW_{(1-x)}S_{2y}Se_{2(1-y)}$ monolayer.

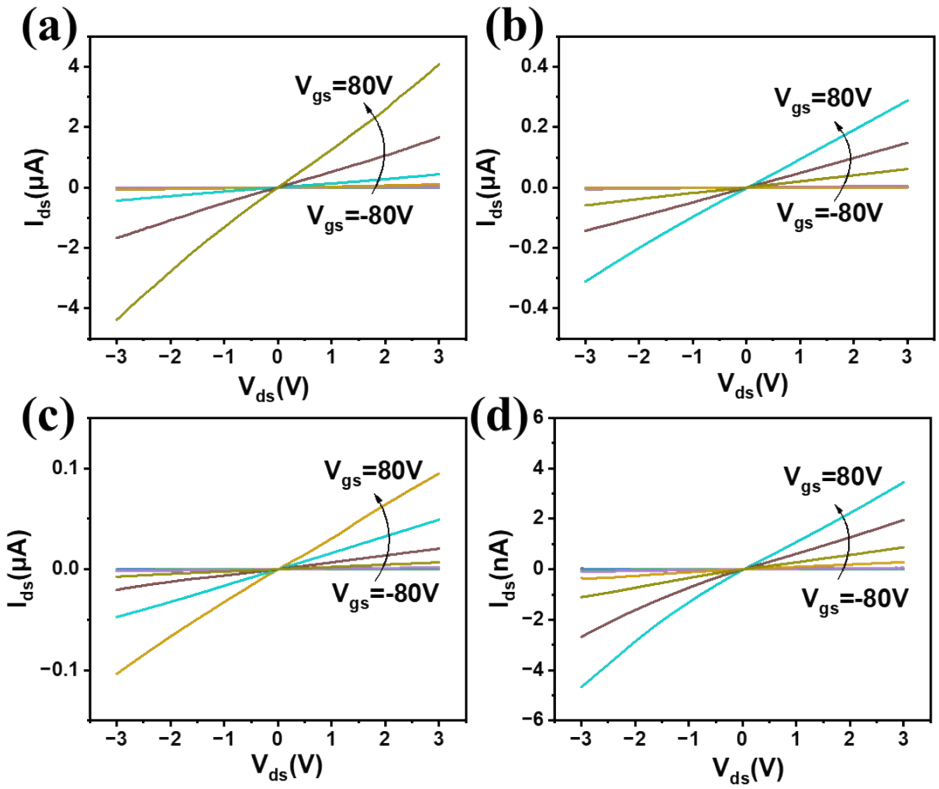

Fig S7 Output curves of $Mo_xW_{(1-x)}S_{2y}Se_{2(1-y)}$ at different growth temperatures: (a) ~825℃, (b) ~850℃, (c) ~875 ℃，(d)~900℃.

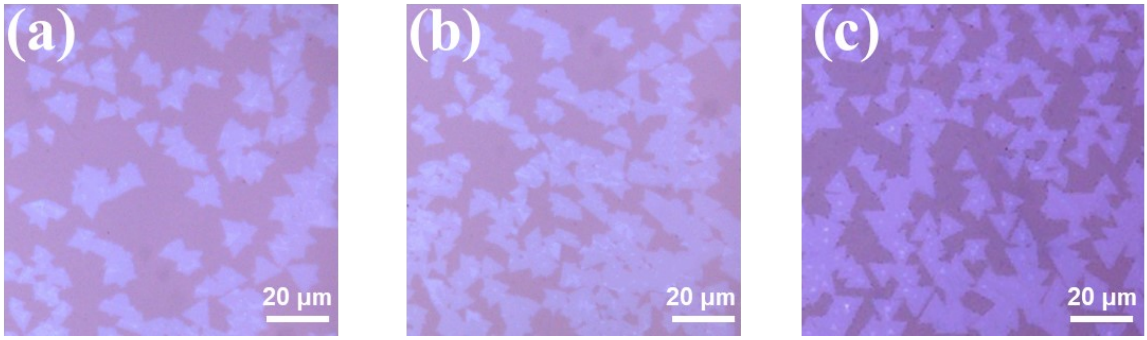

Fig. S8 Optical images of (a) Fe-, (b), Co- (c) Ni-doped $Mo_xW_{(1-x)}S_{2y}Se_{2(1-y)}$.

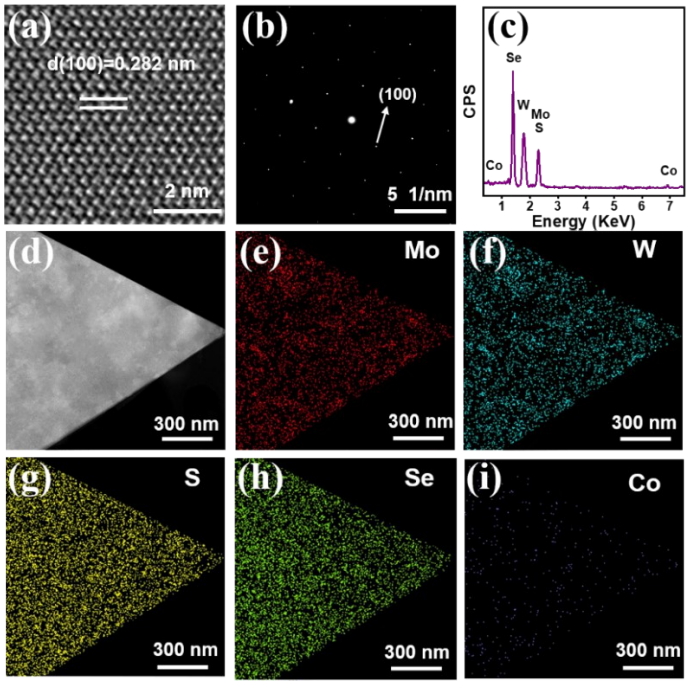

Fig S9 Structural characterization of the Co-doped $Mo_xW_{(1-x)}S_{2y}Se_{2(1-y)}$. (a-i) The HRTEM image, SAED image, EDS elemental analysis, STEM image and EDS mapping images of Co-doped $Mo_xW_{(1-x)}S_{2y}Se_{2(1-y)}$, respectively.

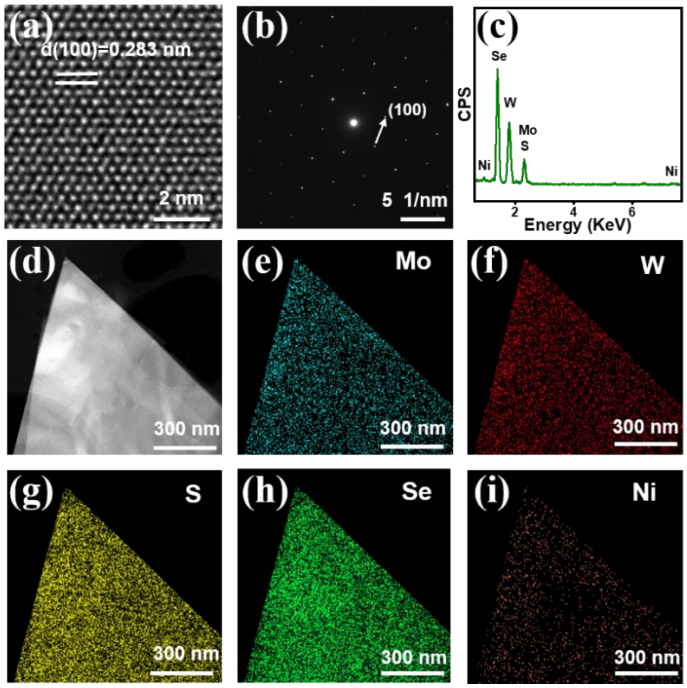

Fig. S10 Structural characterization of the Ni-doped $Mo_xW_{(1-x)}S_{2y}Se_{2(1-y)}$. (a-i) The HRTEM image, SAED image, EDS elemental analysis, STEM image and EDS mapping images of Ni-doped $Mo_xW_{(1-x)}S_{2y}Se_{2(1-y)}$, respectively.

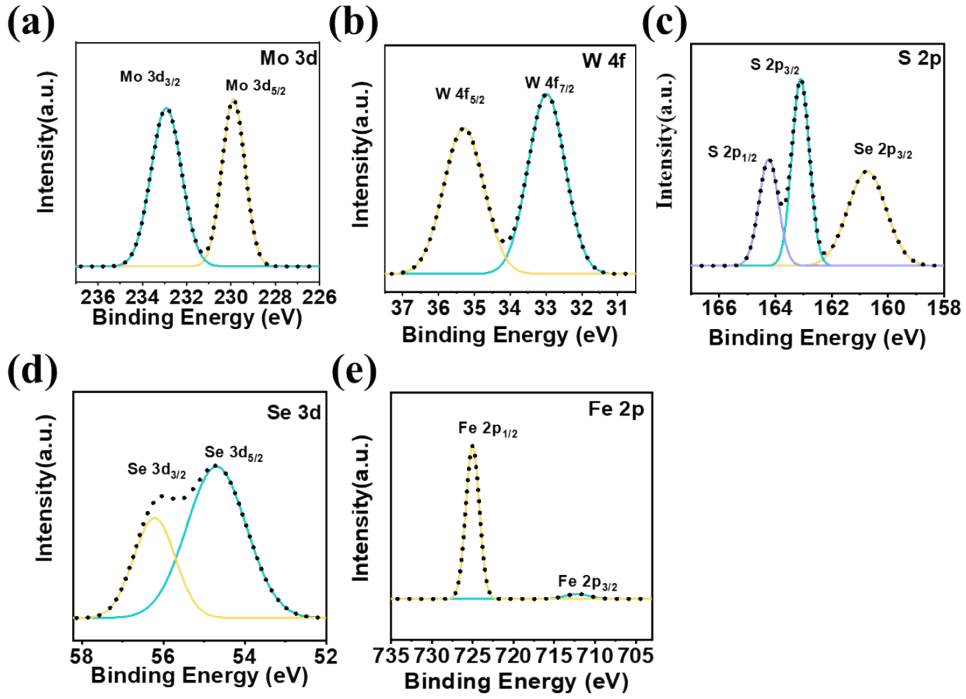

Fig. S11 XPS spectra of as-grown Fe-doped $Mo_xW_{(1-x)}S_{2y}Se_{2(1-y)}$, revealing the 3d, 4f, 2p, 3d, 2p binding states of Mo, W, S , Se and Fe respectively.

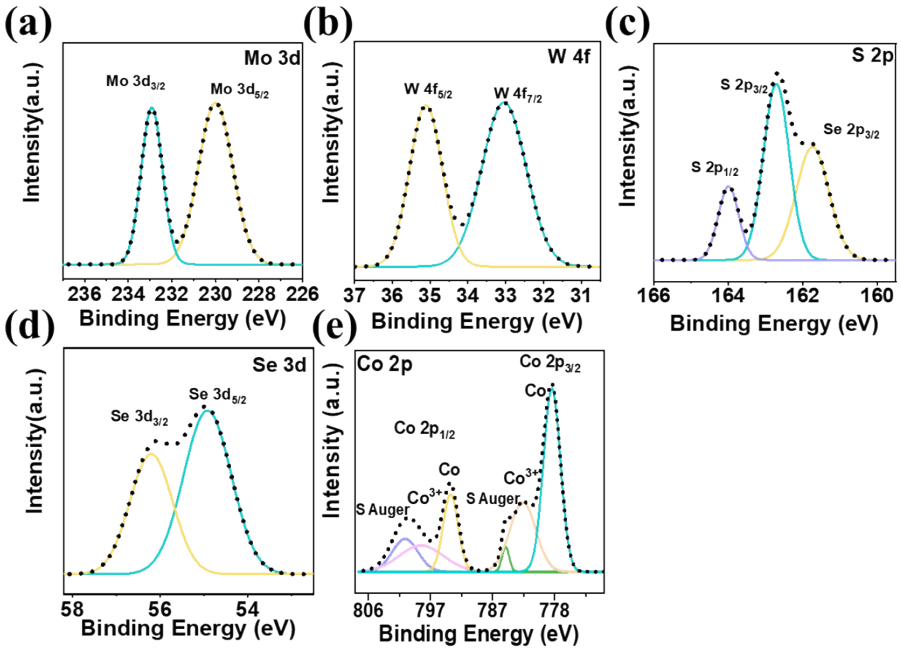

Fig. S12 XPS spectra of as-grown Co-doped $Mo_xW_{(1-x)}S_{2y}Se_{2(1-y)}$, revealing the 3d, 4f, 2p, 3d, 2p binding states of Mo, W, S , Se and Co respectively.

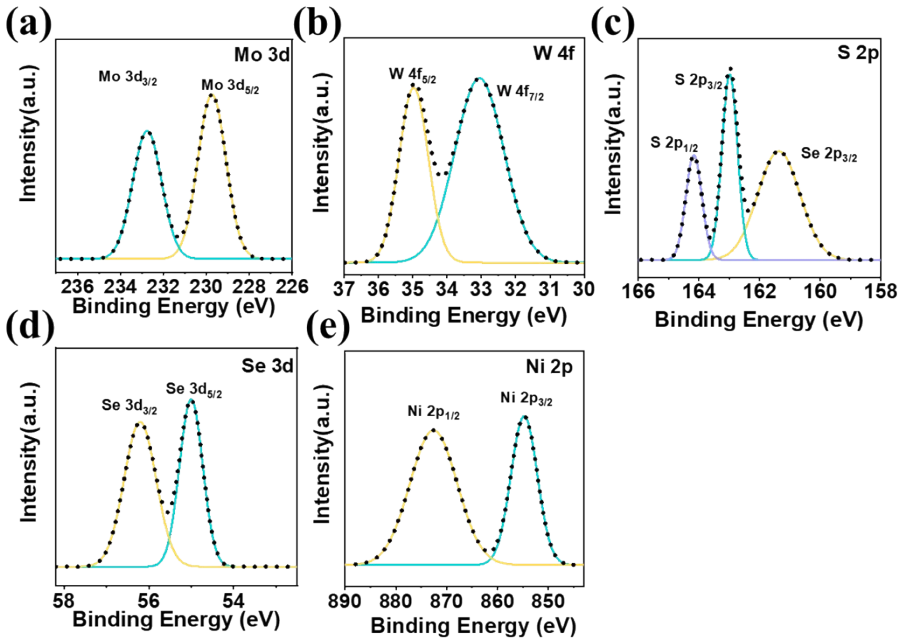

Fig. S13 XPS spectra of as-grown Ni-doped $Mo_xW_{(1-x)}S_{2y}Se_{2(1-y)}$, revealing the 3d, 4f, 2p, 3d, 2p binding states of Mo, W, S , Se and Ni respectively.

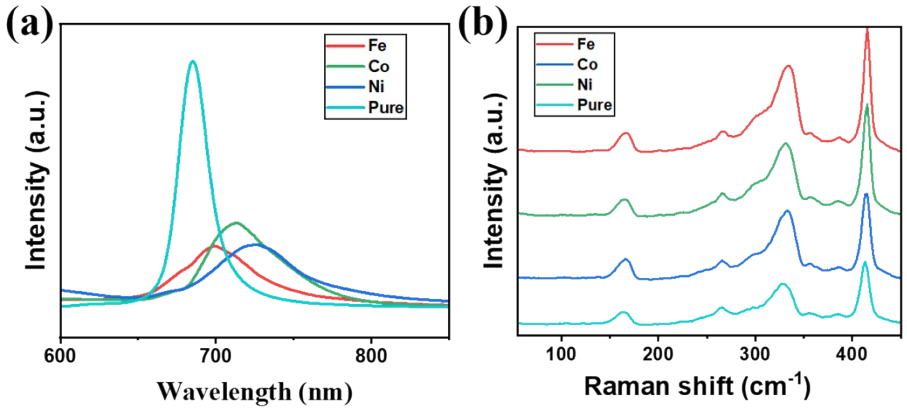

Fig. S14 PL spectra and Raman spectra of as-grown pure and M-doped (Fe, Co, Ni) $Mo_xW_{(1-x)}S_{2y}Se_{2(1-y)}$.

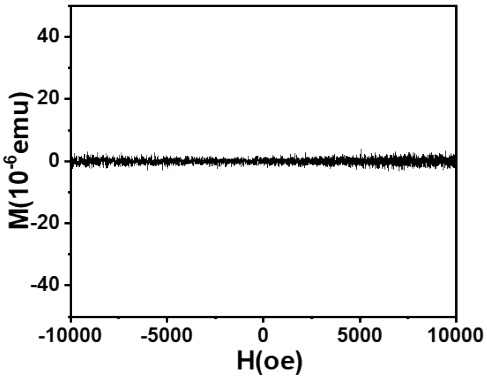

Fig. S15 Magnetic hysteresis loops of pristine $Mo_xW_{(1-x)}S_{2y}Se_{2(1-y)}$.

Temperature (℃)	Atomic Ratio Mo(x)	Atomic Ratio S(y)
825	**0.78**	**0.22**
850	**0.54**	**0.35**
875	**0.67**	**0.49**
900	**0.45**	**0.54**

Tab. S1. Amount of x and y ratio in the as-grown $Mo_xW_{1-x}S_{2y}Se_{2(1-y)}$ alloy.

References:

[1] Hussain, S.; Zhou, R.; Li, Y.; Qian, Z.; Urooj, Z.; Younas, M.; Zhao, Z.; Zhang, Q.; Dong, W.; Wu, Y.; Zhu, X.; Wang, K.; Chen, Y.; Liu, L.; Xie, L. Liquid Phase Edge Epitaxy of Transition-Metal Dichalcogenide Monolayers. *J. Am. Chem. Soc.* 2023, 145, 11348-11355.

[2] Zhang, X.; Cai, X.; Jin, K.; Jiang, Z.; Yuan, H.; Jia, Y.; Wang, Y.; 468 Cao, L.; Zhang, X. Determining the surface tension of two-dimensional nanosheets by a low-rate advancing contact angle measurement. *Langmuir*. 2019, 35, 8308−8315.